Elemental fractionation during LA-ICP-MS analysis of silicate glasses: implications for matrix-independent standardization†

Mabry Gaboardi and Munir Humayun*

Received 16th January 2009, Accepted 11th June 2009
First published as an Advance Article on the web 29th June 2009
DOI: 10.1039/b900876d

To determine the degree to which matrix affects elemental abundance measurements in LA-ICP-MS analysis, and describe these effects in term of elemental properties, we measured elemental sensitivity ratios (ESRs) from a multi-element solution and from the laser ablation of a range of silicate reference materials (SRM 61X series, MPI-DING glasses, USGS basalt glasses). For all analyses, ESRs depend strongly on element mass and first ionization potential (FIP), as expected. For laser ablation of the nearly transparent SRM 612, ESRs show an additional dependence on elemental temperature of condensation (T_c), such that ESRs of refractory elements are lower than predicted by their mass and FIP dependences. To explore the relationship between this volatility dependence and matrix transparency, we exploited the range of transparency available in the SRM 61X series. With increasing transparency of glasses, LA-ICP-MS analyses showed progressive volatility dependence, with measured concentrations of refractory elements being lower, and measured concentrations of volatile elements being higher, than reported concentrations. For the most transparent glass (SRM 614), concentration offsets from the reported concentrations of the refractory and volatile elements were ~20%; for SRM 612 offsets were ~10–15%. We show that this effect is minimized, and possibly negated, by increasing laser energy output. As the offsets for ESRs of refractory elements are uniformly lower in more transparent SRM 612 relative to SRM 610 (11% ± 4%; 1.1 mJ laser energy), successful matrix-independent standardization of refractory elements is possible if the internal normalizing element is approximately the same T_c as the elements to be reported (*e.g.*, Ca and REEs). Volatile elements, however, do not produce uniform ESRs in transparent samples and matrix-independent standardization of volatiles in transparent samples with a 213 nm wavelength laser ablation system will include element-specific systematic errors of the order of tens of percent. All non-transparent glasses analyzed (MPI-DING glasses and USGS BHVO-2G and BCR-2G) show no resolvable matrix-dependent elemental fractionation and may be used interchangeably with an accuracy of better than 10%. In non-transparent samples, the greatest limitation to accurate LA-ICP-MS standardization is the uncertainty in reported reference material concentrations. Matrix-independent standardization of LA-ICP-MS analysis of non-transparent silicates and ceramics, then, is an accurate and viable tool that can best be employed by avoiding calibration with transparent standards, unless using an internal normalizing element of similar T_c to that of the elements to be reported. LA-ICP-MS analysis of transparent silicates and ceramics can be performed at the highest laser energy possible to minimize volatility effects, and calibrated with an internal normalizing element of similar T_c to that of the elements to be reported, using both transparent and non-transparent standards.

Introduction

The combination of laser ablation with inductively coupled plasma mass spectrometry (LA-ICP-MS) provides for the rapid chemical analysis of solid samples (*e.g.*, refs. 1,2) at a spatial resolution better than 100 μm (*e.g.*, refs. 3,4,5). Matrix-dependent inter-element fractionation may occur during LA-ICP-MS analysis due to non-stoichiometric sampling during the ablation process (*e.g.*, refs. 6,7), or the incomplete vaporization of large particles (>125 nm) in the plasma.[8,9,10,11] As standardization in LA-ICP-MS involves both internal and external calibration, matrix-matching of samples and standards has been recommended to correct for these fractionations (*e.g.*, refs. 7,12). Concerns about the necessity for sample-standard matrix-matching, however, limit the possible quantitative applications of the method to specific matrices for which standards are currently available (*e.g.*, silicates, metal), but do not permit the analysis of complex poly-phase materials.

The LA-ICP-MS technique is ideally suited for *in situ* analysis of siderophile and chalcophile elements in meteorites or recently returned cosmic dust samples from the NASA Stardust mission.[13] Flynn *et al.*[14] have analyzed elemental compositions of

Department of Geological Sciences and National High Magnetic Field Laboratory, Florida State University, Tallahassee, FL, 32310-4100, USA. E-mail: humayun@magnet.fsu.edu; Fax: +850-644-0827; Tel: +850-644-1908

† Electronic supplementary information (ESI) available: Tables ESI1–ESI6. See DOI: 10.1039/b900876d

Stardust cometary particles by energy-dispersive synchrotron X-Ray fluorescence analysis (SXRF), but SXRF is not sufficiently sensitive for elements beyond Mo, and cannot analyze elements with atomic number lower than Si in a Si-rich matrix. While most meteorite minerals are Fe-rich, the Stardust grains are embedded in, and intimately fused with, aerogel, the silica-glass collector substrate.[15] Analysis of trace elements in such a silica-dominated matrix has no simple matrix-match, and requires a more thorough knowledge of the nature of matrix-dependent inter-element fractionation.

For much of the history of laser ablation, the NIST SRM 61X series glasses (610, 612, 614, and 616) were the sole available inter-laboratory standards. The SRM 61X series glasses are Na-, Ca-, Al-silicate matrix doped with a wide suite of elements at ~450, ~40, ~1, and ~0.02 ppm, respectively. These glasses range in color from dark blue (SRM 610) to virtually clear (SRM 614 and SRM 616) (Fig. 1), and lack the significant levels of Fe and other transition metals abundant in geological samples. Though SRM 61X series glasses are widely used as LA-ICP-MS standards, they do not provide a suitable matrix match for natural samples. For example, Humayun *et al.*[5] reported systematically lower Ca/Si and Al/Si ratios from SRM 612 relative to the recently available MPI-DING glass reference materials prepared by homogenizing geological materials.[16] Other standard glasses with more geologically appropriate matrices now available include the USGS basalt glasses (BCR-2G, BHVO-2G[17]), and the USGS GSX-1G series reference materials.[18,19] These glasses provide new options for LA-ICP-MS standardization, and allow for the evaluation of the matrix effects introduced by the use of the SRM 61X series.

In this study, we quantify the degree to which matrix affects elemental abundance measurements over a wide range of elements, and describe these effects in terms of elemental properties (mass, first ionization potential (FIP), and volatility). Because such fractionations are pertinent to the accuracy of trace element measurements in geological samples in general, we have performed a systematic study that examines the elemental fractionations in SRM 61X glasses relative to one another, to geologic glass reference materials, and to solution nebulization (SN) ICP-MS standards.

Experimental

All LA-ICP-MS measurements were performed with a New Wave UP 213 laser ablation system coupled to a Thermo Finnigan Element 1™ or Thermo Finnigan Element XR™ ICP-MS at the NHMFL Plasma Analytical Facility.[5] SN-ICP-MS measurements were performed with a Scott-type glass spray chamber equipped with an ESI™ PFA low-flow nebulizer, coupled to the Element XR™. Both mass spectrometers use a series of magnetic mass jumps combined with electrostatic scanning to cover the mass spectrum from masses 6-240.[20,21]

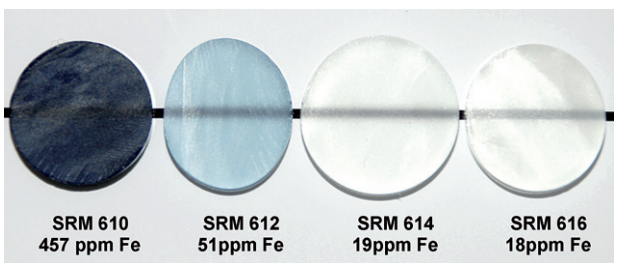

Fig. 1 Systematic increase in transparency with decreasing Fe contents in NIST SRM glasses 610, 612, 614, and 616. The glasses were photographed on a white background with a black ruled line.

Measurement of mass bias curves

To compare mass bias curves obtained by LA-ICP-MS and SN-ICP-MS, we measured peaks over a wide mass range from ^{7}Li to ^{238}U at a mass resolution of 400 (R = 400), as follows: ^{7}Li*, ^{9}Be*, ^{11}B*, ^{23}Na*, ^{25}Mg, ^{27}Al*, ^{29}Si, ^{31}P, ^{43}Ca*, ^{45}Sc, ^{47}Ti, ^{48}Ti, ^{51}V*, ^{53}Cr, ^{55}Mn, ^{57}Fe, ^{59}Co*, ^{60}Ni, ^{65}Cu, ^{66}Zn, ^{71}Ga*, ^{73}Ge, ^{75}As, ^{82}Se*, ^{83}Kr, ^{85}Rb, ^{88}Sr, ^{89}Y, ^{90}Zr, ^{93}Nb, ^{95}Mo*, ^{97}Mo, ^{102}Ru, ^{103}Rh, ^{105}Pd, ^{106}Pd, ^{107}Ag, ^{109}Ag*, ^{111}Cd, ^{115}In, ^{118}Sn, ^{120}Sn, ^{121}Sb, ^{123}Sb, ^{125}Te, ^{126}Te*, ^{133}Cs, ^{138}Ba, ^{139}La, ^{140}Ce, ^{141}Pr, ^{143}Nd, ^{145}Nd*, ^{147}Sm, ^{149}Sm, ^{154}Sm, ^{151}Eu, ^{153}Eu, ^{155}Gd, ^{156}Gd, ^{157}Gd, ^{158}Gd, ^{159}Tb, ^{160}Gd, ^{164}Dy, ^{165}Ho, ^{166}Er, ^{169}Tm*, ^{174}Yb, ^{175}Lu, ^{180}Hf, ^{181}Ta, ^{182}W, ^{185}Re, ^{190}Os, ^{192}Os, ^{193}Ir, ^{195}Pt*, ^{197}Au, ^{205}Tl, ^{208}Pb, ^{209}Bi, ^{232}Th*, ^{238}U. Asterisks denote magnet mass jumps. A Ni–Cu sampler cone and regular Ni skimmer cone were used in measurements of all mass bias curves. When possible, we measured multiple isotopes of an element to correct for molecular and atomic isobaric interferences. SN-ICP-MS measurements were made on two 500 ppt solutions (68A–AB, 68A–AC) produced by dilution of multi-element solutions from High Purity Standards™. Each contained a 2% HNO_3 solution doped with most elements (68A–A), blended with either a solution containing HF-complexed elements (68A–B: Si, Ti, Ge, Zr, Nb, Mo, Ag, Sn, Sb, Te, Hf, Ta, W) or with the platinum group elements (PGEs) in trace HCl (68A–C). Each solution was measured by ICP-MS in triplicate. For solution measurements, background intensities were measured on a procedural blank of 2% HNO_3.

NIST SRM 612 was measured in triplicate with the following laser conditions in line mode: 65 μm spot size, 60% laser energy output (~0.2 mJ), 10 Hz repetition rate, 10 μm/s travel speed. Measurements were made using the same cones, on the Element XR™, with the same method as described above for solutions. ^{48}Ti and ^{69}Ga peaks were discarded due to interferences from ^{48}Ca and ArSi, respectively. Background intensities measured on Ar gas blanks during the measurement session were subtracted from sample intensities.

Additionally, BCR-2G and SRM glasses 616, 614, 612, and 610 were each measured using the same cones, method, and blank correction described above, but with the Element 1™. BCR-2G was measured in triplicate with the following laser conditions in line mode: 65 μm spot size, 75% laser energy output (~0.4 mJ), 10 Hz repetition rate, 10 μm/s travel speed. Each SRM glass was measured once with the following laser conditions in line mode: 100 μm spot size, 100% laser energy output (~1.1 mJ), 20 Hz repetition rate, 10 μm/s travel speed. To explore the effect of laser energy output, SRM 612 was then measured with a lower energy output (75%; ~0.7 mJ) while all other parameters were held constant. To compare spot versus line modes, SRM 612 was measured using spot mode ablation, with spot size and laser energy as above (100 μm spot size, 100% laser energy output) and a repetition rate of 10 Hz, so as not to penetrate deeply into the sample during the 2 minutes of sampling time.

Atomic isobaric interferences of ^{48}Ca, ^{82}Kr, and ^{164}Er were stripped from ^{48}Ti, ^{82}Se, and ^{164}Dy. Oxide corrections to middle rare earth elements (REEs) were performed by solving simultaneous linear equations using the multiple isotopes measured for these elements. Since oxide formation can measurably reduce the peak intensities of Ba, La, Ce, Pr, Th and U, the measured intensities for these elemental peaks were corrected for losses due to oxide formation, as follows. Measured intensities of ThO and UO were added to measured Th and U intensities. Intensities of $^{135, 137, 138}$BaO, ^{139}LaO, ^{140}CeO, and ^{141}PrO were obtained from the ^{151}Eu, ^{153}Eu, ^{154}Sm, ^{155}Gd, ^{156}Gd, and ^{157}Gd isotopes and included with the Ba, La, Ce, and Pr peaks. Nearly all isobaric corrections for isotopes included in elemental ESRs were $\leq 6\%$ for solutions and $\leq 6\%$ for LA-ICP-MS analyses of silicate glasses (most were <2%). The only exceptions included Th in solution (16%) and ^{153}Eu in BCR-2G (11% from ^{137}Ba^{16}O). All isotope intensities were converted to elemental sensitivity ratios (ESRs):

$$ESR_x = \frac{(I/f)_i/(I/f)_{r_i}}{C_x/C_{r_x}} \quad (1)$$

where I is the peak intensity, f is the isotopic abundance, C is the concentration of the element, i is the isotope measured of element x, and r_i is the isotope measured of the internal normalizing element r_x. We averaged ESRs of multiple isotopes measured on the same element (available as ESI Tables ESI1 and ESI2†). Abundances for most elements in SRM 610 and 612 were taken from Pearce *et al.*;[22] trace elements are from their "preferred values". Concentrations of elements certified by NIST are used when available (Mn (in 610), Fe, Ni, Rb, Sr, Ag, Pb, Th, and U). Re, Au, and Pt concentrations are taken from Sylvester and Eggins.[23] Abundances for most elements in BCR-2G were taken from Jochum and Nohl.[24] All others were retrieved from GeoReM,[25] as were all elemental abundances for SRMs 614 and 616.[26,27]

ESRs measured from SRM 610 (Table ESI2†) were used to calibrate element concentrations in SRMs 612, 614, and 616 from analyses performed on the Element 1™. Detection limits were calculated from 3 standard deviations of the background intensities.

Measurement of matrix effects in silicate glasses

We measured elemental abundances in geologic glasses comprising a wide range of Fe concentrations as follows: NIST SRM 612, MPI-DING glasses (ATHO-G (rhyolite), StHs6/80-G (andesite), T1-G (quartz diorite), KL2-G (basalt), ML3B-G (basalt), and GOR128-G (komatiite)), and USGS basalt glasses BHVO-2G and BCR-2G. All measurements were performed on the Element 1™. These measurements were made in preparation for analysis of the NASA Stardust material, so Ni–X skimmer cones were used to decrease mass bias, enhancing measured intensities of low mass peaks. Since isobaric interferences measured by LA-ICP-MS on the SRM and geologic glasses above were typically <2% we did not correct for them in further analyses.

We analyzed low mass isotope peaks (^{23}Na, ^{24}Mg, ^{27}Al, ^{29}Si, ^{31}P, ^{44}Ca, ^{45}Sc, ^{47}Ti, ^{51}V, ^{52}Cr, ^{55}Mn, ^{56}Fe, ^{59}Co, ^{60}Ni, ^{63}Cu, ^{66}Zn, ^{69}Ga) in medium resolution (R = 4000) to avoid molecular isobaric interferences, and high mass isotope peaks (^{88}Sr, ^{89}Y, ^{90}Zr, ^{93}Nb, ^{120}Sn, ^{138}Ba, ^{139}La, ^{140}Ce, ^{141}Pr, ^{144}Nd, ^{147}Sm, ^{153}Eu, ^{164}Dy, ^{166}Er, ^{174}Yb, ^{180}Hf, ^{181}Ta, ^{208}Pb, ^{232}Th, ^{238}U, plus ^{29}Si) in low resolution (R = 400). As operating conditions vary for each reference material, they are reported in ESI (Table ESI3†) for all R = 4000 measurements. All R = 400 measurements were performed in two sessions (corresponding to Sessions 1 and 2 in Table ESI3†) Conditions for all Session 1 R = 400 measurements were as follows: line ablation, 30–40 μm spot size, 50% laser energy output, 10 Hz repetition rate, 10 μm/s travel speed, laser energy ~0.1 mJ. Session 2 conditions were: spot ablation (2 minutes of ablation), 55–80 μm spot size, 50% laser energy output, 10 Hz repetition rate, laser energy ~0.1–0.2 mJ. Background intensities, measured on Ar gas blanks during the measurement session, were subtracted from sample isotope intensities, which were converted to Si-normalized ESRs (available in ESI as Table ESI4†), as above. Jochum *et al.*[16] report MPI-DING concentrations. Abundances for most elements in BHVO-2G are compiled by the USGS; all others were retrieved from GeoReM.[28] ESRs from ML3B-G were used to calibrate concentrations for the other reference materials listed in Table ESI4.†

Results

Mass bias curves, first ionization potentials, and volatility

For the two multi-element solutions measured (68A–AB, 68A–AC), the peaks for elements in common between the solutions reproduced within 2% on average (with the exception of Li and Al peaks at ~28% offset, due to high background), so ESRs calculated from triplicate measurements for each solution are given in Table ESI1† as a single average, and shown as a single mass bias curve (Fig. 2a). Solution ESRs of multiple isotopes of each poly-isotopic element were averaged, as they reproduced to within 4% for most elements, with the following exceptions. Silver, Te, and Nd isotopes were each separated by a magnet mass jump that produced an offset of about 15%, but are still presented as a single average. Sodium, Si, P, Ca, and Fe peaks were compromised by high backgrounds and are not included in the solution data in Table ESI1.† For LA-ICP-MS measurements of BCR-2G (Fig. 2b) and SRM 612 (Fig. 2c), isotope reproducibility is comparable to the solution results described above. The average relative standard deviation (RSD, 1σ) for triplicate ESRs within a reference material is 3.5%. Titanium is not included in the SRM 612 data presented as both isotopes measured were compromised by interferences. Other elements not included in Table ESI1† for SRM 612 or BCR-2G lacked reliable concentration information.

In Fig. 2, elements are coded according to their FIP. It should be noted that elements with the highest FIPs (circles; > 8 eV) have much lower ESRs than elements of similar mass with lower FIPs. The solution mass bias curve (solid line in Fig. 2a) is then defined by the linear regression for elements with FIPs below 7 eV (diamonds). The overall distribution of these elements is outlined by the dashed field, which was then superposed on Figs. 2b–c, to show the analogous results for LA-ICP-MS analysis of BCR-2G and SRM 612, respectively. Although BCR-2G was analyzed on an Element 1 and the solution and SRM

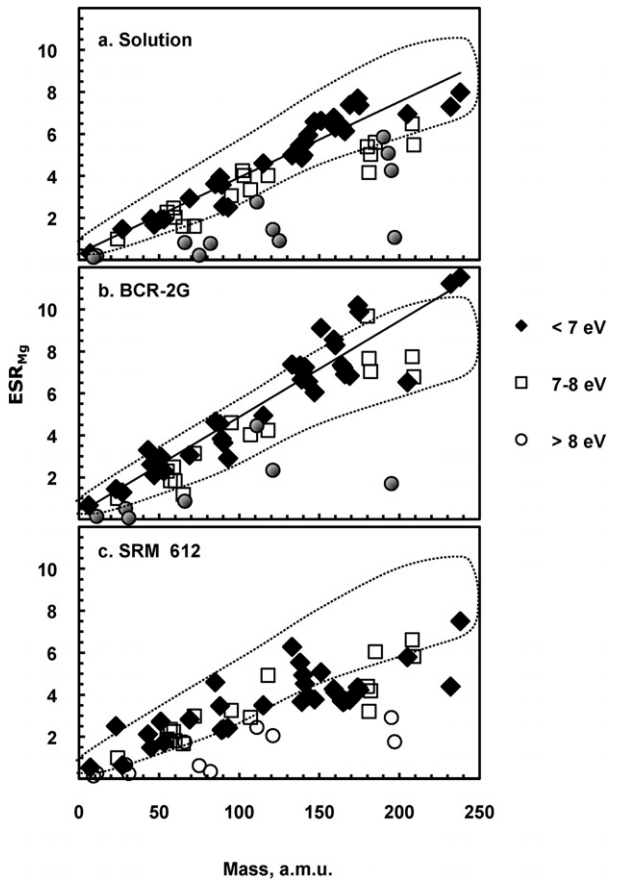

Fig. 2 Mg-normalized ESRs for multi-element solution (a) produce a mass bias curve defined by elements with FIP < 7 eV. Higher FIP elements fall below the curve. Elements in BCR-2G (b) measured by LA-ICP-MS produce similar ESRs and mass bias curve, but LA-ICP-MS measurements of SRM 612 (c) show more element scatter. The dashed field, outlining the overall distribution of < 7 eV elements measured by SN-ICP-MS (a), was superposed on (b, c) for comparison. Data in Table ESI1.† All analyses were performed in triplicate. Error bars (1σ) are not included as they are smaller than symbols, averaging 3.5%.

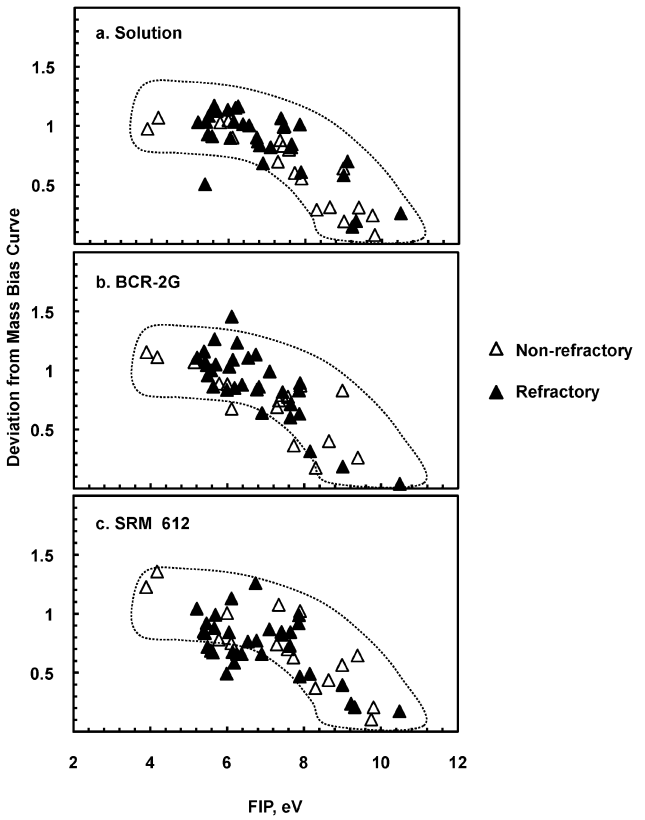

Fig. 3 The deviations from mass bias curves (Fig. 2) versus FIP, with elements coded according to T_c. For SN-ICP-MS (a) there is clear dependence on FIP, around which a dashed outline was drawn. The outline does not quite capture the lowest mass element, Li, which is the only obvious outlier. When this outline is superposed on LA-ICP-MS data (b,c) the same dependence on FIP is observable, with an additional dependence for SRM 612 (c) on volatility in which many elements with high T_c have intensities lower than predicted by their FIP dependence. For SRM 612 the deviation of Na (2.18) falls above the scale of the plot.

612 measurements were performed on an Element XR, the slopes of the solution mass bias curve and the BCR-2G curve are similar. For elements with FIP < 7 eV, it can be seen that these elements define comparable linear regression lines (solid lines in Figs 2a–b), and the two data sets plot largely within the same dashed field. In contrast, many of the ESRs for SRM 612 fall below the dashed field, and a linear regression does not represent the trend of the elements with FIP < 7 eV. As both the solution measurements and the LA-ICP-MS measurements of SRM 612 were made on the Element XR with the same cone configuration (cones had not been removed between measurements), this result is not due to changes in instrumental configuration.

For each element in Fig. 3, the deviation between the measured ESR and the ESR calculated from the mass bias curve is plotted against the FIP. For SRM 612, the mass bias curve used to calculate ESRs was obtained from the solution data. In Fig. 3, elements are coded according to temperature of condensation (T_c) with solid symbols representing refractory elements (elements with high condensation temperatures), and open symbols representing elements with low condensation temperatures (see "Volatility" in Discussion for further details).

For SN-ICP-MS data (Fig. 3a) the deviation clearly depends on FIP, with the exception of Li, an obvious outlier. The dashed field defines the crude trend of FIP-dependent deviation for the solution ESRs. This dashed field is then superposed on the LA-ICP-MS results from BCR-2G (Fig. 3b) and SRM 612 (Fig. 3c). The BCR-2G results overlap the FIP trend defined by the solution results, as do the non-refractory elements in SRM 612 (open symbols), with exception of Na. Many refractory elements in SRM 612, however, plot below this dashed field. Thus, for SRM 612 there is an additional dependence on volatility in which many refractory elements have ESRs lower than predicted by their FIP and mass bias alone. As will be seen below, the refractory depletion observed in SRM 612 is also characteristic of other low-Fe glasses of this series, the causes of which are explored in the Discussion.

ESRs for SRM 610 (~457 ppm Fe), SRM 612 (~51 ppm Fe), SRM 614 (~19 ppm Fe), and SRM 616 (~18 ppm Fe) are reported in Table ESI2.† Isotope reproducibility was 5% or better in SRM 610, SRM 612 and SRM 614, but was poorer in

SRM 616, as the lower concentrations resulted in higher error. Beryllium, P, Sc, Ti, Cr, Mn, Fe, Co, and Ni, are not included in Table ESI2† in cases when the blanks were more than half of the measured sample intensities. It should be noted that due to the low, and sometimes poorly known, concentrations in SRM 616, ESRs for several elements are likely inaccurate and are provided for comparison only.

Matrix effects in silicate glasses

For the purpose of determining the matrix dependence of the ESRs, a series of measurements were performed on a wide range of silicate matrices, from geologic glasses to SRM 612. In the course of routine measurements of major and trace elements in our laboratory, ESRs on Al and Ca in SRM 612, MPI-DING, and USGS glasses were obtained. To explore the generic and reproducible nature of the matrix effects seen in Figs. 2c and 3c, this broader data set is summarized in Table ESI3.† Because Al, Si, and Ca are major elements in all the silicate glasses, their ESRs are the most precisely measured. Further, both Al and Ca are refractory elements of FIP < 7 eV with masses below 50. Since Si has, relative to Al and Ca, an intermediate mass, high FIP, and low T_c, any depletion of Al and Ca measured intensities (*i.e.* lower ESRs) should be due to the T_c of Al and Ca. This makes Al and Ca ideal elements for pinpointing a matrix-dependent "volatility effect" in LA-ICP-MS.

In Fig. 4, these Al ESRs are plotted against Ca ESRs, with each symbol shape corresponding to a different measurement session, all performed with X-cones. Open symbols represent ESRs measured from geologic glasses; closed symbols are SRM 612 measurements. Generally, within a given measurement session, MPI-DING glasses and USGS glasses produce similar ESRs, while SRM 612 ESRs are lower. The relative error (1σ) on a linear regression through all points is 4%. Thus, correlated matrix effects as seen in Fig. 4 demonstrate the matrix dependence of LA-ICP-MS ESRs for refractory elements, particularly in the case of SRM 612 in comparison to other geologic glasses. It should be noted, however, that the three highest SRM 612 ESRs, which are comparable to the ESRs of geologic glasses, were measured at higher laser energies than were the other SRM 612 ESRs. The effect of laser energy on ESRs is explored further in the Discussion.

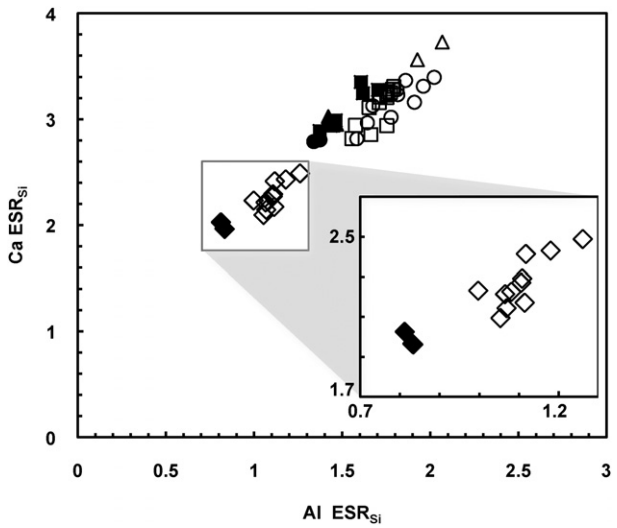

Fig. 4 Si-normalized ESRs for SRM 612 (solid) and for a variety of other standards (MPI-DING series, BHVO-2G, BCR-2G; open). Shapes (diamond, circle, square, and triangle) correspond to measurements sessions, so that SRM 612 measurements may be compared to those of other standards measured on the same day. For example, the inset includes ESRs from SRM 612 and other geologic glasses measured during analytical session 4. Laser settings, which vary between measurements, and data, are reported in Table ESI3.†

Table ESI4† contains ESRs measured for the comparison of silicate glasses, using X-cones. Each ESR is the average of multiple analyses (2–6). Some reference materials (SRM 612, ATHO-G, StHs6/80-G, ML3B-G and GOR128-G) were measured during at least two sessions; others (T1-G, BCR-2G, and BHVO-2G) were measured during one session only. Across reference materials, the RSD (1σ) of the ESRs for a given element averages 7%. This does not include less reliable ESRs: those measured on elements whose reported concentrations are only information values, on elements with reported concentrations < 0.1 ppm, and for elements whose measured concentrations are more than 35% lower than their reported concentrations (Ni and Co in ATHO-G). Elements with across-element ESR RSDs > 10% include Cr, Ni, Sn, and Hf.

Table ESI5† contains ESRs measured on ML3B-G during three different analytical sessions. ESR reproducibility improves with element concentration, such that ESRs from the most abundant elements (>1000 ppm) are consistent to within 8%.

Measured concentrations of geologic glasses were calibrated against ML3B-G ESRs and are reported in Table ESI6.† With the exception of GOR128-G, for which much lower trace element concentrations introduce greater error (RSD average 9%), the average RSD (1σ) for measured elemental abundances in geologic glasses is 4%.

Discussion

Elemental fractionation in LA-ICP-MS analysis

In SN-ICP-MS, intensities are converted to concentrations with empirically determined constants, which vary from element to element according to mass and FIP. For high resolution ICP-MS, intensity/concentration ratios plotted against element masses produce a characteristically linear mass bias regression, with high FIP elements systematically plotting below the mass bias regression line.[20] For the instrumental conditions of the present study, this is shown in Fig. 2a for solution nebulization of a 500 ppt solution, and in Fig. 2b for laser ablation of BCR-2G. To demonstrate the FIP effect, we have plotted the deviation from the linear mass bias curve against the FIP in Fig. 3, with both solution (Fig. 3a) and laser ablation ICP-MS of BCR-2G (Fig. 3b) yielding identical patterns. By contrast, LA-ICP-MS analysis of SRM 612 (Figs. 2c, 3c) fails to conform to patterns seen for SN-ICP-MS and LA-ICP-MS, suggesting that, for some samples, elemental response is dependent on an additional factor: elemental temperature of condensation, shown in Fig. 3 by using separate symbols for refractory and volatile elements. If elements in all LA-ICP-MS analyses depended only on mass bias and FIP, as documented here for BCR-2G, then

matrix-independent conversion of intensities to concentrations could confidently be applied for all samples, and calibration against solution should produce accurate results (*e.g.*, refs. 29,30). Fractionation recorded in SRM 612, however, demonstrates that in some cases matrix does affect LA-ICP-MS measurements. Matrix-dependent fractionations during LA-ICP-MS analysis have been reported elsewhere, such that samples with different matrices displayed dissimilar elemental fractionations.[5,12]

There are at least two sources that may contribute significantly to the volatility effect observed here in SRM 612 (Figs. 2c, 3c): non-stoichiometric sampling at the site of ablation (*e.g.*, ref. 6) and incomplete vaporization of particles in the ICP-MS plasma.[10,11] During ablation with an excimer (193 nm) laser, Eggins *et al.*[6] documented systematic changes in the ratio of volatile to refractory elements, while ablating for long durations at a single spot (thousands of pulses per spot). A similar effect was noted by Campbell and Humayun[4] and Mank and Mason[31] for continuous ablation at a single spot with 266 nm and 248 nm laser systems. These later workers recommended ablating with a crater depth to diameter ratio near unity[4] or less than six[31] to avoid elemental fractionation associated with continuous ablation at a single spot. Accordingly, in the present study we avoided deep pits and acquired continuous data in line scan mode or in shallow spots. Thus, elemental fractionation observed in this study must largely be due to effects other than non-stoichiometric sampling.

Aeschliman *et al.*[10] provide direct evidence of the incomplete vaporization in the ICP-MS plasma of large particles produced by the laser ablation of Y_2O_3 pellets. During ablation with each 266 nm and 193 nm laser wavelengths, particles were photographed streaking through the plasma, hitting the cones. Kuhn and Günther[11] further examined the source of elemental fractionation for a 266 nm laser system by collecting the ablated material from SRM 610 in three size fractions (total aerosol, particles <340 nm, and particles <125 nm) and measuring their compositions by SN-ICP-MS. Though the total aerosol was representative of the sample ablated, indicating that sampling was stochiometric, there was a size-related dependence on ablated particle composition. Specifically, the smallest fraction (particles <125 nm) showed a >20% enrichment in the following elements: Na, V, Ni, Cu, Zn, Ga, Rb, Ag, Cd, In, Tl, Pb, Bi, and U. Despite stoichiometric sampling of material in their study, Kuhn and Günther[11] found elemental fractionation in their LA-ICP-MS measurements and concluded that incomplete vaporization of large particles in the ICP-MS plasma was the primary source of the observed elemental fractionation. This incomplete vaporization of large particles in the ICP-MS plasma, then, is the most likely cause of the low refractory ESRs we measure for SRM 612 by LA-ICP-MS.

Volatility

Several workers have used melting points or boiling points of the pure element or of simple oxides as a proxy for volatility of an element without achieving much success in relating elemental behavior during laser ablation with these parameters.[9,11] To assess the role of volatility in elemental fractionation during laser ablation ICP-MS, deviations from reported concentrations are plotted in Fig. 5 as a function of the nebular condensation temperature in the solar nebula, T_c.[32] Unlike melting or boiling points of pure elements or simple element oxides, the condensation temperatures reflect the thermodynamic interactions of a multi-component oxide-silicate system.[33] The choice of nebular T_c for ordering the elements is somewhat arbitrary but no quantitative measure of volatility during laser ablation is presently available. It is, therefore, not surprising that several elements appear as anomalies in our measured volatility trend (*e.g.*, Re, W, U, Mo). If anomalies were observed in only one reference material, it could arguably be due to inaccuracy in reported concentrations; however since both reference materials display systematic deviations for these elements, the anomaly is likely intrinsic to that element's fractionation behavior. These elements (Mo, Re, W, and U) are notable as their volatilities are strongly dependent on their redox state. In a reducing gas (*i.e.*, under the nebular conditions for which the condensation temperatures were calculated) Mo, Re, and W condense as refractory metals. However, the gas composition formed during ablation is dominated by the oxygen-rich vapor released by the breakdown of these silicate glasses. Indeed, Wang *et al.*[34] reported that during the thermal decomposition of a Ca–Mg–Al-silicate glass in vacuum, oxygen released by the break-down of silicates locally increased the oxygen fugacity around the experimental charge, resulting in the oxidation of elements sensitive to redox changes (Ce, in their experiment). Rhenium, W, and Mo, then, may vaporize as their volatile oxides[35] in the plasma. The change in redox state results in a lower temperature of condensation/evaporation for these elements. Volatile loss of these elements was documented for Mo and W in the solar nebula,[36] and for Re from subaerial lavas (*e.g.*, ref. 37,38). For U, possible volatilization from impact-generated silicate melts (tektites) has been reported.[39,40] It seems likely, then, that our observed anomalies in Re, W, Mo, and U, are simply the result of incorrect positioning along our x-axis. In the absence of better quantification of their volatile behavior, we note that these anomalies can be explained by the systematically more volatile nature of these elements, but we currently lack a T_c with which to better assign the element in Fig. 5.

Factors that affect the accuracy of LA-ICP-MS analysis

Transparency. We explore this observed volatility dependence further by exploiting the range of transparencies in the SRM 61X series (Fig. 1). Laser energy does not easily couple with transparent samples at 213 nm, since a substantial fraction of the laser energy is transmitted deep into the sample, resulting in larger particles. If more transparent glasses produce larger particles in the aerosol (*e.g.*, refs. 8,41) and larger particles are incompletely vaporized in the ICP-MS plasma,[10] then the depletion of refractory elements observed in SRM 612 in Fig. 3c should be more apparent in a more transparent glass. In Fig. 5, the degree of this volatility effect is observed to be correlated with glass transparency, such that the depletion of refractory elements is progressively larger in the order: SRM 614 > SRM 612 > SRM 610. Although we have not measured SRM 610 against one of the more Fe-rich glasses, SRM 610 may also exhibit some of this volatility effect seen prominently in SRM 612 and SRM 614. Though deviations for SRM 616 are not included in Fig. 5, they

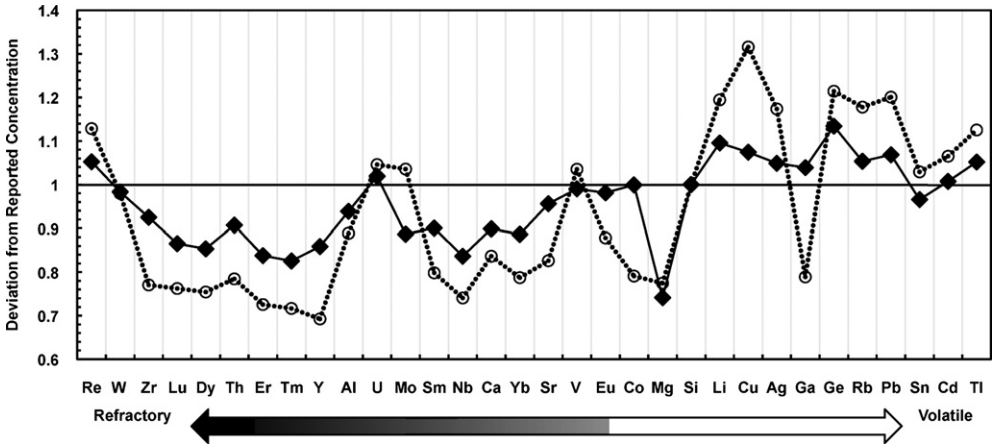

Fig. 5 Deviations are measured concentrations divided by reported concentrations for SRM 612 (solid diamonds; ~51 ppm Fe) and SRM 614 (open circles; ~19 ppm Fe) calibrated against SRM 610 (~457 ppm Fe). With notable exceptions, volatile element enrichment and refractory element depletion are more pronounced with decreasing Fe content of the glass. ESRs are listed in Table ESI2.†

are roughly similar to those of SRM 614. (For SRM 616, deviations of measured concentrations from reported concentrations can be calculated for each element by dividing the SRM 616 ESR by the SRM 610 ESR; Table ESI2.†) This is expected as SRM 616 and SRM 614 have comparable Fe concentrations, and are about equally transparent in the optical region (Fig. 1). The use of these transparent NIST SRM glasses as standards for calibrating laser ablation ICP-MS measurements at wavelengths even as low as 213 nm, then, introduces unnecessary error to the measurement of concentrations in geologic samples.

Mode of ablation. To explore laser parameters that might affect the accuracy of elemental concentrations, we varied separately the mode of ablation and the laser energy used to sample SRM 612. In Fig. 6a, we plot the deviations from reported concentrations in SRM 612 for measurements ablated with line mode (solid squares) and spot mode (open circles). Spot size and laser energy were kept constant. There is no clear change in deviation from reported concentration due to ablation mode on spots with shallow craters. The elemental fractionation, however, persists in both modes and is clearly reproduced.

Laser energy. Fig. 6b displays deviations from reported SRM 612 concentrations for measurements performed with a higher laser energy (1.1 mJ; closed squares) and a lower laser energy (0.7 mJ; open circles). For lower energy measurements, deviations are greater by ~5% for many elements, with deviations following the volatility pattern seen in Fig. 5. This strengthening of the volatility pattern is small compared to the effect of glass transparency, but is clearly a cause of increased deviation from reported concentrations.

In Fig. 7, SRM 612 concentrations, calibrated against ML3B-G ESRs (Table ESI5†), are plotted as deviations from reported concentrations. Open circles represent SRM 612 measured at least twice during each of three analytical sessions at ~50% laser energy output (~0.3 mJ). Solid diamonds are the averages of three measurements from the same analytical session at a higher energy (70% laser energy output, ~1.2 mJ). Both sets of measurements were made at R = 4000. RSDs (1σ) for measured concentrations are ≤ 7% (average 4%) for the low energy setting (~0.3 mJ) and ≤ 4% (average 2%) for the higher energy setting (~1.2 mJ), except for Zn, which has RSDs of 15% and 9%, respectively. Interestingly, in Fig. 7, SRM 612 measured at higher laser energy shows no clear volatility trend and better

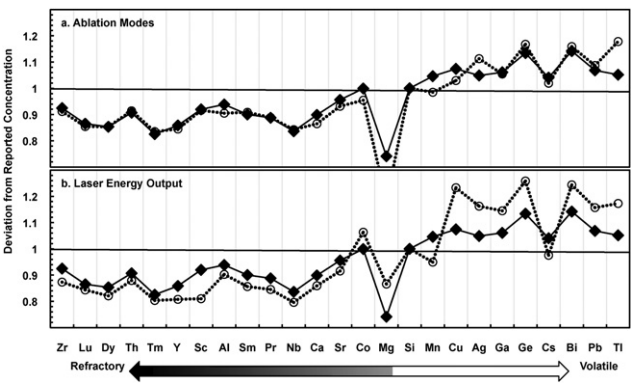

Fig. 6 SRM 612 calibrated against SRM 610 under different operating conditions. (a) Ablation modes: line (solid diamonds) versus spot (open circle). (b) Laser energy output: high (1.1 mJ; solid) versus low (0.7 mJ; open).

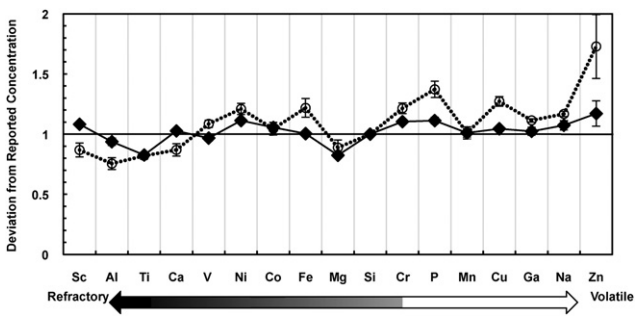

Fig. 7 SRM 612 calibrated against ML3B-G. Open circles are the average of concentrations measured on three days at ~50% laser energy output (average 0.3 mJ); solid diamonds are the average of three measurements on the same day with 70% laser output (1.2 mJ). Error bars are 1σ.

RSDs than measurements performed at lower energy. Thus, volatility effects in transparent glasses diminish, and may disappear, with increasing laser energy output. This is consistent with the idea that volatility effects are caused by incomplete vaporization of large particles in the ICP-MS plasma. Any variable (*e.g.*, transparency, laser energy, laser wavelength[41]) resulting in poor laser-sample coupling apparently contributes to a volatility effect. Above a certain threshold of coupling, however, that variable should no longer cause matrix-dependent volatility effects.

Uncertainty in reported concentrations. In order to explore the effects of matrix-dependence in LA-ICP-MS, we measured concentrations of 37 elements across a wide suite of silicate matrices. Using ESRs from ML3B-G for calibration, we measured the elemental abundances for USGS, MPI-DING, and SRM 612 glasses (Table ESI6†). For selected reference materials representing the broad range of compositions observed in geological glasses, deviations from reported concentrations are plotted in Fig. 8. For all geologic glasses analyzed, nearly all measured elemental concentrations are within 10% of the reported concentrations (average 7%). The deviations are not dependent on silicate matrix, as rhyolite (ATHO-G) elemental abundances calibrated against a basalt (ML3B-G) are no farther offset than elemental abundances of a komatiite (GOR128-G) calibrated against the same basalt. In Fig. 8, those elements that deviate by an amount substantially greater than the precision of the measurements generally have larger uncertainties on their reported concentrations (Fig. 9). This has the important corollary that future improvements in obtaining certified values for elements in these reference materials will result in substantial improvements in the accuracy of future LA-ICP-MS analyses. Thus, for Fe-bearing glasses, matrix-independent standardization is a reliable calibration method at the level of accuracy currently available.

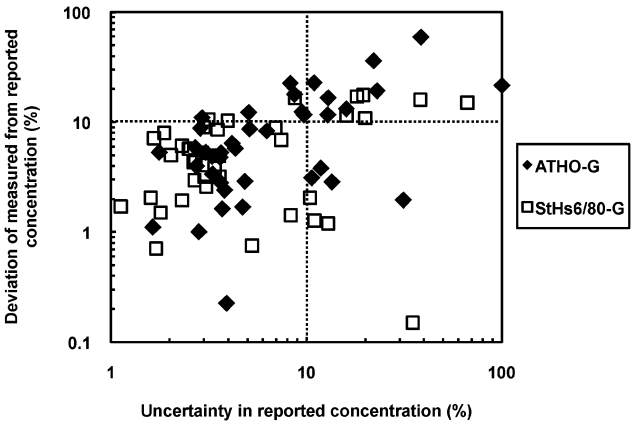

Fig. 9 For geologic glasses, deviations between measured and reported concentrations > 10% are typically associated with > 10% uncertainties in reported concentrations.

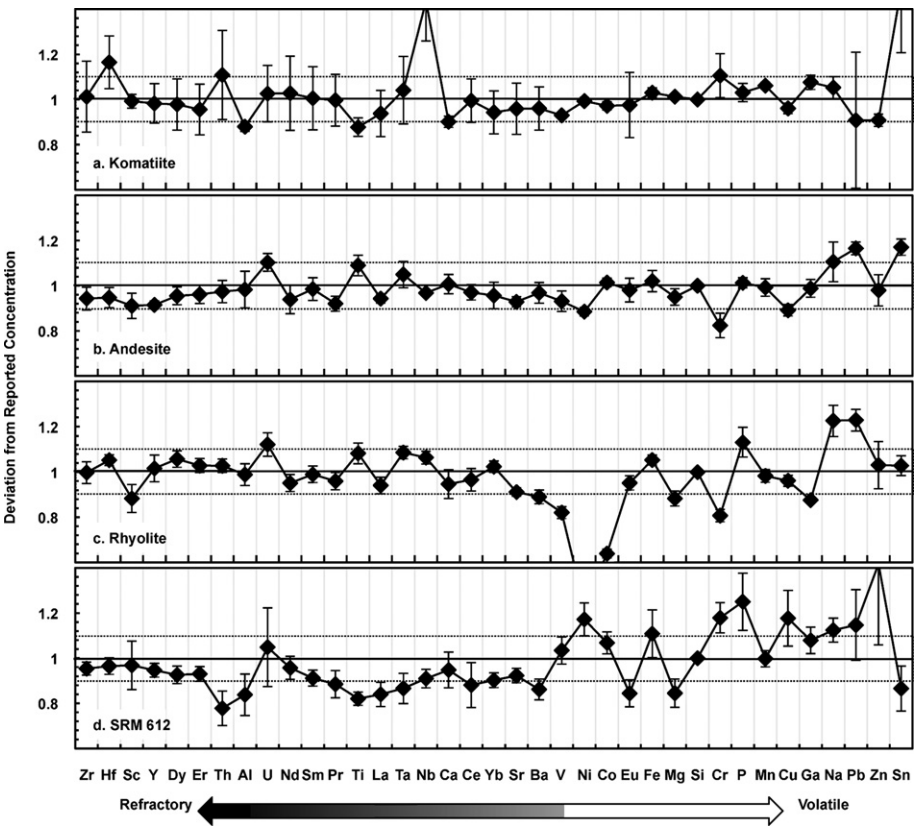

Fig. 8 For each silicate glass standard (a: GOR128-G, b: StHs6/80-G, c: ATHO-G, d: SRM 612) deviations are measured concentrations (Table ESI6†) of selected elements divided by reported concentrations cited in text. All measured concentrations are calibrated against basalt ML3B-G. Error bars are 1σ of the average of at least 4 analyses during two measurement sessions. ESRs for each standard are reported in Table ESI4.†

Strategies for matrix-independent standardization

Below, we summarize the strategies for standardization that provide the best accuracies for LA-ICP-MS analysis of silicates or ceramics attainable with a 213 nm laser ablation system. These strategies may also apply more broadly to other matrices, such as metals or sulfides.

• Matrix-independent standardization is accurate across a wide range of matrices with the exception of transparent standards.

Deviations of elements in SRM 612 in Figs. 5, 6, and 8 are generally greater than in the geologic glasses (Fig. 8) and display a characteristic volatility fractionation. Thus, at the settings used in this study, sample transparency is the most obvious cause of the observed matrix-dependent elemental fractionation. SRM 61X glasses, then, are inappropriate standards for Fe-bearing silicate glasses and may result in the reporting of inappropriately high refractory element concentrations and low volatile element concentrations. In most cases, it is preferable to select for standardization MPI-DING glasses, USGS basalt glasses, or the newly available GSX-1G glasses[18,19] produced at the USGS, which have a high-iron basaltic matrix doped with a wide suite of elements. Selecting a reference material with a matrix that readily absorbs laser radiation should negate possible LA-ICP-MS induced volatility effects, and allow for matrix-independent calibration of samples to within the accuracy achievable with currently available reference materials.

• Choice of internal normalizing element becomes important to standardize between transparent and non-transparent materials.

If it is necessary to use SRM 61X glasses as standards, or if samples to be measured are transparent, it is important to choose for internal normalization an element of similar T_c to that of the other elements measured. In the analysis of USGS glasses by Strnad *et al.*[42] calibration of refractory elements against mid-T_c element Si produced concentrations systematically higher than a calibration against refractory Ca. Tanaka *et al.*[43] avoided the problem by normalizing rare earth elements (REEs) to Ca, all refractory elements, and measured concentrations within 10% using both calcite reference materials and SRM 61X glasses. Because refractory elements produce uniformly lower ESRs in SRM 612 relative to SRM 610 (11% ± 4%; Table ESI2†), the choice of a refractory element for normalization results in much more accurate measured refractory concentrations. This explains why some previous calibrations against SRM glasses have been successful (*e.g.*, refs. 3,43). Volatile elements, however, produce more variable ESRs and matrix-independent standardization for volatile elements in transparent glasses results in lower accuracies of measured concentrations. Some geochemical studies require the characterization of both volatile and refractory elements, for example in geochronology the Rb/Sr and U/Pb ratios need to be simultaneously determined with great accuracy. In these cases the best accuracy can only be achieved by calibration against non-transparent reference materials.

• Ablating transparent samples at the highest laser energy possible decreases volatility effects.

Finally, when measuring transparent glasses, it is desirable to ablate with the highest possible laser energy settings to improve laser-sample coupling and decrease measured volatility effects (Fig. 7). During the analysis of some complex poly-phase materials, as in laser ablation of cometary materials embedded in the silica aerogel, the ablation of transparent materials is unavoidable. In this case, ablation with high laser energy settings should produce the most accurate LA-ICP-MS calibration attainable, negating or minimizing volatility effects.

Conclusion

ESRs measured from a multi-element solution (SN-ICP-MS) and from the laser ablation (LA-ICP-MS) of BCR-2G and SRM 612 depend strongly on element mass and FIP. ESRs measured on the transparent NIST SRM 61X series glasses show an additional dependence on elemental temperature of condensation, such that ESRs of refractory elements are lower, and ESRs of volatile elements are higher, than predicted by their mass and FIP dependences. This matrix-dependent elemental fractionation intensifies in more transparent glasses, and we measure as much as ~20% offsets between reported and measured element concentrations in our most transparent glass (SRM 614). We show that these offsets can be minimized or negated by ablating with high laser energy. Non-transparent glasses show no resolvable matrix- dependent volatility effects and may be employed interchangeably for calibration, without regard for matrix. For many elements in non-transparent glasses, uncertainties in reported reference material concentrations are the greatest obstacle in accuracy of LA-ICP-MS measurement. For the measurement of transparent samples, reliable matrix-independent calibration of refractory elements is possible when the T_c of the internal normalizing element approximately matches that of the elements to be determined (*e.g.*, Ca for REEs). The widespread use of the transparent NIST SRM 61X series glasses has caused much of the concern regarding matrix matching in LA-ICP-MS, but the availability of many new reference materials with an Fe-rich matrix now make possible the wider use of LA-ICP-MS as an analytical tool.

Acknowledgements

This research was supported by the NASA Cosmochemistry Program (NNG06GF50G). We thank two anonymous reviewers for their helpful comments.

References

1 A. L. Gray, *Analyst*, 1985, **110**, 551–556.
2 P. Arrowsmith, *Anal. Chem.*, 1987, **59**, 1437–1444.
3 M. D. Norman, N. J. Pearson, A. Sharma and W. L. Griffin, *Geostand. Newsl.*, 1996, **20**, 247–261.
4 A. J. Campbell and M. Humayun, *Anal. Chem.*, 1999, **71**, 939–946.
5 M. Humayun, S. B. Simon and L. Grossman, *Geochim. Cosmochim. Acta*, 2007, **71**, 4609–4627.
6 S. M. Eggins, L. P. J. Kinsley and J. M. G. Shelley, *Appl. Surf. Sci.*, 1998, **129**, 278–286.
7 J. Kosler, M. Wiedenbeck, R. Wirth, J. Hovorka, P. Sylvester and J. Mikova, *J. Anal. At. Spectrom.*, 2005, **20**, 402–409.
8 M. Guillong and D. Gunther, *J. Anal. At. Spectrom.*, 2002, **17**, 831–837.
9 I. Rodushkin, M. D. Axelsson, D. Malinovsky and D. C. Baxter, *J. Anal. At. Spectrom.*, 2002, **17**, 1231–1239.
10 D. B. Aeschliman, S. J. Bajic, D. P. Baldwin and R. S. Houk, *J. Anal. At. Spectrom.*, 2003, **18**, 1008–1014.
11 H. R. Kuhn and D. Gunther, *J. Anal. At. Spectrom.*, 2004, **19**, 1158–1164.

12 K. P. Jochum, B. Stoll, K. Herwig and M. Willbold, *J. Anal. At. Spectrom.*, 2007, **22**, 112–121.
13 D. Brownlee, P. Tsou, J. Aleon, C. M. O. Alexander, T. Araki, S. Bajt, G. A. Baratta, R. Bastien, P. Bland, P. Bleuet, J. Borg, J. P. Bradley, A. Brearley, F. Brenker, S. Brennan, J. C. Bridges, N. D. Browning, J. R. Brucato, E. Bullock, M. J. Burchell, H. Busemann, A. Butterworth, M. Chaussidon, A. Cheuvront, M. F. Chi, M. J. Cintala, B. C. Clark, S. J. Clemett, G. Cody, L. Colangeli, G. Cooper, P. Cordier, C. Daghlian, Z. R. Dai, L. D'Hendecourt, Z. Djouadi, G. Dominguez, T. Duxbury, J. P. Dworkin, D. S. Ebel, T. E. Economou, S. Fakra, S. A. J. Fairey, S. Fallon, G. Ferrini, T. Ferroir, H. Fleckenstein, C. Floss, G. Flynn, I. A. Franchi, M. Fries, Z. Gainsforth, J. P. Gallien, M. Genge, M. K. Gilles, P. Gillet, J. Gilmour, D. P. Glavin, M. Gounelle, M. M. Grady, G. A. Graham, P. G. Grant, S. F. Green, F. Grossemy, L. Grossman, J. N. Grossman, Y. Guan, K. Hagiya, R. Harvey, P. Heck, G. F. Herzog, P. Hoppe, F. Horz, J. Huth, I. D. Hutcheon, K. Ignatyev, H. Ishii, M. Ito, D. Jacob, C. Jacobsen, S. Jacobsen, S. Jones, D. Joswiak, A. Jurewicz, A. T. Kearsley, L. P. Keller, H. Khodja, A. L. D. Kilcoyne, J. Kissel, A. Krot, F. Langenhorst, A. Lanzirotti, L. Le, L. A. Leshin, J. Leitner, L. Lemelle, H. Leroux, M. C. Liu, K. Luening, I. Lyon, G. MacPherson, M. A. Marcus, K. Marhas, B. Marty, G. Matrajt, K. McKeegan, A. Meibom, V. Mennella, K. Messenger, S. Messenger, T. Mikouchi, S. Mostefaoui, T. Nakamura, T. Nakano, M. Newville, L. R. Nittler, I. Ohnishi, K. Ohsumi, K. Okudaira, D. A. Papanastassiou, R. Palma, M. E. Palumbo, R. O. Pepin, D. Perkins, M. Perronnet, P. Pianetta, W. Rao, F. J. M. Rietmeijer, F. Robert, D. Rost, A. Rotundi, R. Ryan, S. A. Sandford, C. S. Schwandt, T. H. See, D. Schlutter, J. Sheffield-Parker, A. Simionovici, S. Simon, I. Sitnitsky, C. J. Snead, M. K. Spencer, F. J. Stadermann, A. Steele, T. Stephan, R. Stroud, J. Susini, S. R. Sutton, Y. Suzuki, M. Taheri, S. Taylor, N. Teslich, K. Tomeoka, N. Tomioka, A. Toppani, J. M. Trigo-Rodriguez, D. Troadec, A. Tsuchiyama, A. J. Tuzzolino, T. Tyliszczak, K. Uesugi, M. Velbel, J. Vellenga, E. Vicenzi, L. Vincze, J. Warren, I. Weber, M. Weisberg, A. J. Westphal, S. Wirick, D. Wooden, B. Wopenka, P. Wozniakiewicz, I. Wright, H. Yabuta, H. Yano, E. D. Young, R. N. Zare, T. Zega, K. Ziegler, L. Zimmerman, E. Zinner and M. Zolensky, *Science (Washington, D.C.)*, 2006, **314**, 1711–1716.
14 G. J. Flynn, P. Bleuet, J. Borg, J. P. Bradley, F. E. Brenker, S. Brennan, J. Bridges, D. E. Brownlee, E. S. Bullock, M. Burghammer, B. C. Clark, Z. R. Dai, C. P. Daghlian, Z. Djouadi, S. Fakra, T. Ferroir, C. Floss, I. A. Franchi, Z. Gainsforth, J. P. Gallien, P. Gillet, P. G. Grant, G. A. Graham, S. F. Green, F. Grossemy, P. R. Heck, G. F. Herzog, P. Hoppe, F. Horz, J. Huth, K. Ignatyev, H. A. Ishii, K. Janssens, D. Joswiak, A. T. Kearsley, H. Khodja, A. Lanzirotti, J. Leitner, L. Lemelle, H. Leroux, K. Luening, G. J. MacPherson, K. K. Marhas, M. A. Marcus, G. Matrajt, T. Nakamura, K. Nakamura-Messenger, T. Nakano, M. Newville, D. A. Papanastassiou, P. Pianetta, W. Rao, C. Riekel, F. J. M. Rietmeijer, D. Rost, C. S. Schwandt, T. H. See, J. Sheffield-Parker, A. Simionovici, I. Sitnitsky, C. J. Snead, F. J. Stadermann, T. Stephan, R. M. Stroud, J. Susini, Y. Suzuki, S. R. Sutton, S. Taylor, N. Teslich, D. Troadec, P. Tsou, A. Tsuchiyama, K. Uesugi, B. Vekemans, E. P. Vicenzi, L. Vincze, A. J. Westphal, P. Wozniakiewicz, E. Zinner and M. E. Zolensky, *Science (Washington, D.C.)*, 2006, **314**, 1731–1735.
15 M. E. Zolensky, T. J. Zega, H. Yano, S. Wirick, A. J. Westphal, M. K. Weisberg, I. Weber, J. L. Warren, M. A. Velbel, A. Tsuchiyama, P. Tsou, A. Toppani, N. Tomioka, K. Tomeoka, N. Teslich, M. Taheri, J. Susini, R. Stroud, T. Stephan, F. J. Stadermann, C. J. Snead, S. B. Simon, A. Simionovici, T. H. See, F. Robert, F. J. M. Rietmeijer, W. Rao, M. C. Perronnet, D. A. Papanastassiou, K. Okudaira, K. Ohsumi, I. Ohnishi, K. Nakamura-Messenger, T. Nakamura, S. Mostefaoui, T. Mikouchi, A. Meibom, G. Matrajt, M. A. Marcus, H. Leroux, L. Lemelle, L. Le, A. Lanzirotti, F. Langenhorst, A. N. Krot, L. P. Keller, A. T. Kearsley, D. Joswiak, D. Jacob, H. Ishii, R. Harvey, K. Hagiya, L. Grossman, J. N. Grossman, G. A. Graham, M. Gounelle, P. Gillet, M. J. Genge, G. Flynn, T. Ferroir, S. Fallon, D. S. Ebel, Z. R. Dai, P. Cordier, B. Clark, M. F. Chi, A. L. Butterworth, D. E. Brownlee, J. C. Bridges, S. Brennan, A. Brearley, J. P. Bradley, P. Bleuet, P. A. Bland and R. Bastien, *Science (Washington, D.C.)*, 2006, **314**, 1735–1739.
16 K. P. Jochum, B. Stoll, K. Herwig, M. Willbold, A. W. Hofmann, M. Amini, S. Aarburg, W. Abouchami, E. Hellebrand, B. Mocek, I. Raczek, A. Stracke, O. Alard, C. Bouman, S. Becker, M. Ducking, H. Bratz, R. Klemd, D. de Bruin, D. Canil, D. Cornell, C. J. de Hoog, C. Dalpe, L. Danyushevsky, A. Eisenhauer, W. R. Premo, W. D. D. Sun, M. Tiepolo, R. Vannucci, T. Vennemann, D. Wayne and J. D. Woodhead, *Geochem. Geophys. Geosyst.*, 2006, **7**, 1–44.
17 R. Wolf and S. Wilson, *USGS reference materials program*, USGS, Fact Sheet 2007–p. 3056.
18 M. Guillong, K. Hametner, E. Reusser, S. A. Wilson and D. Gunther, *Geostand. Geoanal. Res.*, 2005, **29**, 315–331.
19 K. P. Jochum, M. Willbold, I. Raczek, B. Stoll and K. Herwig, *Geostand. Geoanal. Res.*, 2005, **29**, 285–302.
20 I. Feldmann, W. Tittes, N. Jakubowski, D. Stuewer and U. Giessmann, *J. Anal. At. Spectrom.*, 1994, **9**, 1007–1014.
21 U. Giessmann and U. Greb, *Fresenius' J. Anal. Chem.*, 1994, **350**, 186–193.
22 N. J. G. Pearce, W. T. Perkins, J. A. Westgate, M. P. Gorton, S. E. Jackson, C. R. Neal and S. P. Chenery, *Geostand. Newsl.*, 1997, **21**, 115–144.
23 P. J. Sylvester and S. M. Eggins, *Geostand. Newsl.*, 1997, **21**, 215–229.
24 K. P. Jochum and U. Nohl, *Chem. Geol.*, 2008, **253**, 50–53.
25 K. P. Jochum and F. Nehring, GeoReM, BCR-2G GeoReM preferred values, 7/2008, (http://georem.mpch-mainz.gwdg.de).
26 K. P. Jochum and F. Nehring, GeoReM, SRM 614 GeoReM preferred values, 7/2008, (http://georem.mpch-mainz.gwdg.de).
27 K. P. Jochum and F. Nehring, GeoReM, SRM 616 GeoReM preferred values, 7/2008, (http://georem.mpch-mainz.gwdg.de).
28 K. P. Jochum and F. Nehring, GeoReM, BHVO-2G GeoReM preferred values, 7/2008, (http://georem.mpch-mainz.gwdg.de).
29 J. J. Leach, L. A. Allen, D. B. Aeschliman and R. S. Houk, *Anal. Chem.*, 1999, **71**, 440–445.
30 D. B. Aeschliman, S. J. Bajic, D. P. Baldwin and R. S. Houk, *J. Anal. At. Spectrom.*, 2003, **18**, 872–877.
31 A. J. G. Mank and P. R. D. Mason, *J. Anal. At. Spectrom.*, 1999, **14**, 1143–1153.
32 K. Lodders, *Astrophys. J.*, 2003, **591**, 1220–1247.
33 L. Grossman, *Geochim. Cosmochim. Acta*, 1972, **36**, 597–619.
34 J. H. Wang, A. M. Davis, R. N. Clayton, T. K. Mayeda and A. Hashimoto, *Geochim. Cosmochim. Acta*, 2001, **65**, 479–494.
35 R. C. Weast, M. J. Astle, W. H. Beyer and Chemical Rubber Company, *CRC handbook of chemistry and physics: a ready-reference book of chemical and physical data*, CRC Press, Boca Raton, Fla. 1985.
36 B. Fegley and H. Palme, *Earth Planet. Sci. Lett.*, 1985, **72**, 311–326.
37 V. C. Bennett, M. D. Norman and M. O. Garcia, *Earth Planet. Sci. Lett.*, 2000, **183**, 513–526.
38 J. C. Lassiter, *Earth Planet. Sci. Lett.*, 2003, **214**, 311–325.
39 J. T. Wasson, X. W. Ouyang and W. K. Stovall, *Meteoritics*, 1990, **25**, 419.
40 J. T. Wasson, *Earth Planet. Sci. Lett.*, 1991, **102**, 95–109.
41 M. Guillong, I. Horn and D. Gunther, *J. Anal. At. Spectrom.*, 2003, **18**, 1224–1230.
42 L. Strnad, M. Mihaljevic and O. Sebek, *Geostand. Geoanal. Res.*, 2005, **29**, 303–314.
43 K. Tanaka, Y. Takahashi and H. Shimizu, *Anal. Chim. Acta*, 2007, **583**, 303–309.